Petroleum Science 22 (2025) 684–696

Contents lists available at ScienceDirect

Petroleum Science

journal homepage: www.keaipublishing.com/en/journals/petroleum-science

Original Paper

Effects of multi-scale wave-induced fluid flow on seismic dispersion, attenuation and frequency-dependent anisotropy in periodic-layered porous-cracked media

Zhao-Yun Zong [a, *], Yan-Wen Feng [b], Fu-Bin Chen [a, c], Guang-Zhi Zhang [a]

[a] State Key Laboratory of Deep Oil and Gas, China University of Petroleum (East China), Qingdao, 266580, Shandong, China
[b] Shale Gas Research Institute, PetroChina Southwest Oil & Gas Field Company, Chengdu, 610051, Sichuan, China
[c] Centre for Exploration Geophysics, Curtin University, Perth, WA 6845, Australia

ARTICLE INFO

Article history:
Received 5 May 2024
Received in revised form
5 July 2024
Accepted 11 November 2024
Available online 13 November 2024

Edited by Meng-Jiao Zhou

Keywords:
Wave-induced fluid flow
Multi-scale wave equations
Anisotropy
Dispersion and attenuation

ABSTRACT

The wave-induced fluid flow (WIFF) occurring in the ubiquitous layered porous media (e.g., shales) usually causes the appreciable seismic energy dissipation, which further leads to the frequency dependence of wave velocity (i.e., dispersion) and elastic anisotropy parameters. The relevant knowledge is of great importance for geofluid discrimination and hydrocarbon exploration in the porous shale reservoirs. We derive the wave equations for a periodic layered transversely isotropy medium with a vertical axis of symmetry (VTI) concurrently with the annular cracks (PLPC medium) based on the periodic-layered model and anisotropic Biot's theory, which simultaneously incorporate the effects of microscopic squirt fluid flow, mesoscopic interlayer fluid flow and macroscopic global fluid flow. Notably, the microscopic squirt shorten fluid flow emerges between the annular-shaped cracks and stiff pores, which generates one attenuation peak. Specifically, we first establish the stress-strain relationship and pore fluid pressure in a PLPC medium, and then use them to derive the wave equations by means of the Newton's second law. The plane analysis is implemented on the wave equations to yield the analytic solutions for phase velocities and attenuation factors of four waves, namely, fast P-wave, slow P-wave, SV-wave and SH-wave, and the anisotropy parameters can be therefore computed. Simulation results show that P-wave velocity have three attenuation peaks throughout the full frequency band, which respectively correspond to the influences of interlayer flow, the squirt flow and the Biot flow. Through the results of seismic velocity dispersion and attenuation at different incident angles, we find that the WIFF mechanism also has a significant impact on the dispersion characteristics of elastic anisotropy parameters within the low-mid frequency band. Moreover, it is shown that several poroelastic parameters, such as layer thickness ratio, crack aspect ratio and crack density have notable influence on seismic dispersion and attenuation. We compare the proposed modeled velocities with that given by the existing theory to confirm its validity. Our formulas and result can provide a better understanding of wave propagation in PLPC medium by considering the unified impacts of micro-, meso- and macro-scale WIFF mechanisms, which potentially lays a theoretical basis of rock physics for seismic interpretation.

1. Introduction

When seismic wave propagates in the fluid-saturated fractured media, velocity dispersion and energy attenuation will occur due to the multi-scale heterogeneity inside the media (Krzikalla and Müller, 2011; Mukerji and Mavko, 1994; Parra and Xu, 1994; Sharma, 2004; Zhang et al., 2019). The seismic attenuation, dispersion and frequency-dependent anisotropy contain the abundant information of the properties of subsurface reservoir rocks and pore fluids, which can be used for effective hydrocarbon interpretation and reservoir characterization in seismic exploration (Wang et al., 2022; Zhang et al., 2017). Meanwhile, the influence of fractures on seismic wave attenuation and dispersion provides a potential tool to quantitatively detect the content and distribution

* Corresponding author.
E-mail address: zongzhaoyun@upc.edu.cn (Z.-Y. Zong).

https://doi.org/10.1016/j.petsci.2024.11.006

of fractures in subsurface fractured media (Amalokwu et al., 2016; Li et al., 2018a, 2018b; Wei et al., 2013; Wang et al., 2018). Nevertheless, the quantitative seismic evaluation of reservoir is based on the comprehensive research of the intrinsic relationship between the physical properties of rocks and seismic attributes.

In order to establish the relationship between the rock physical properties and their dispersion and attenuation, a large quantity of attenuation theories for fluid-saturated poroelastic media are well established, which can be classified into three main categories according to the scales of attention: macroscopic, mesoscopic and microscopic scale (Müller et al., 2010). Biot (1956) introduced an internal energy dissipation mechanism due to viscous fluid flow, widely known as Biot dissipation theory, to develop the two-phase medium theory of wave propagation in porous media containing uniform fluid and then generalized it to the anisotropic case. Nevertheless, the assumption of pore homogeneity in Biot's theory makes its predicted wave energy dissipation of the seismic frequency band much smaller than the experimental observed result (Batzle et al., 2001; Pride et al., 2004). Diverse theories and description methods have been developed for the pore distribution inhomogeneity and the corresponding local fluid flow. One is the microscopic squirt flow mechanism that tend to cause high-frequency dispersion and attenuation, but it is still insufficient to characterize the wave propagation behaviors within the seismic frequencies (Chen et al., 2022; Dvorkin et al., 1995; Diallo et al., 2003; Gurevich et al., 2010; Mavko and Nur, 1979; Subramaniyan et al., 2015; Wu et al., 2020). Fluid flow induced by mesoscopic mechanism can explain many important phenomena in rock physics at the lower frequencies, which has attracted the widespread attention. A series of mesoscopic models have been established, such as the patchy-saturated porous media, the periodic-layered model, the double-porosity model and the improvement of these models (Ba et al., 2011; Chapman, 2003; Chen et al., 2023; Dutta and Ode, 1979; Gurevich and Lopatnikov, 1995; Liao et al., 2023; Pang and Stovas, 2020; Sharma, 2007; Sun et al., 2016; Wei et al., 2013; White, 1975; White et al., 1975), and it is found that the wave dispersion induced by fluid flow at the mesoscopic scale is able to qualitatively explain the wave attenuation at the seismic frequency band. Further considering the coexistence of pores and cracks in real rocks, several authors developed the unified rock physics theory for coexisting pore-cracks and the periodic-layered crack-fracture media theory to interpret the wave attenuation and dispersion in fluid-saturated fracture rocks at a wide range of frequencies (Krzikalla and Müller, 2011; Sun, 2021; Tang et al., 2012; Wang et al., 2023; Yang and Zhang, 2002).

The directional arrangement of fractures or cracks in rocks will cause the underground medium to have anisotropic characteristics, thereby changing the stiffness properties of the rocks and affecting the elastic wave velocity of the rocks. Seismic wave propagation has anisotropic characteristics due to the medium anisotropy, and it is of great significance to analyze the effect of fracture fluids on the anisotropy of seismic waves. To characterize the elastic parameters of fractured rocks, a large amount of WIFF (wave-induced fluid flow) mechanisms containing the fluid flow between the fracture and the rock background developed to describe the frequency dependence of rock properties at seismic frequencies (Chapman, 2009; Chen et al., 2022; Hudson et al., 1996; Kong et al., 2013; Lissa et al., 2019; Meng and Wei, 2021; Sayers and Kachanov, 1995; Shuai et al., 2020; Solovyev et al., 2023). Guo et al. (2019) developed an approximate theoretical model for seismic wave dispersion, attenuation, and frequency-dependent anisotropy in the layered porous media based on Biot's poroelastic theory. Xu et al. (2021) proposed an analytic method to compute the wave dispersion and attenuation for fracture-bearing rocks with anisotropic background. Most current anisotropic seismic wave attenuation and dispersion studies are based on single or double scales of fluid flow, the integrated consideration for velocity dispersion and attenuation and frequency-dependent anisotropy in multiple frequency band will be helpful to better understand the wave propagation in fractured-porous media caused by WIFF (Li and Yan, 2023; Xu et al., 2022).

In the present study, we construct a PLPC (periodic-layered porous-cracked) medium model concurrently incorporating macro-, meso-, and micro-scale WIFF mechanisms based on the Biot's poroelasticity theory, where the microscopic squirt flow occurs between the annular-shaped cracks and stiff pores. Meanwhile, the constitutive matrix and the wave equation for the PLPC model are derived and solved with Newton's second law to obtain the wave velocity and the corresponding attenuation factor. To characterize the frequency-dependent anisotropy, we calculate and analyze the variation characteristics of the Thomsen anisotropy parameters with frequency and crack density. In conclusion, the characteristics of seismic wave attenuation, dispersion of the PLPC model are studied, the validity of the proposed model is confirmed by comparing the modeled velocities with those given by the existing theories, and the influences of different parameters on seismic wave attenuation and dispersion is analyzed.

2. Theory

The PLPC model presents a periodic layered structure, and each layer contains horizontally oriented cracks, which form an annular-shaped pore-crack structure with the stiff pores of the background medium, as shown in Fig. 1. Two layers are selected for amplification, the length is l_1, the width is l_2, the upper layer thickness is X_1, saturated by water, and the lower layer saturated by oil/gas, the total thickness is X_2, but the relative porosity of the upper and lower layers is the same. There is only one type of pore-crack structure in each layer, namely the annular-shaped crack, as shown in Fig. 2. In the PLPC model, the microscopic squirt flow effect occurs between pores and cracks, the mesoscopic interlayer flow effect occurs between the upper and lower layers, and the fluid in the background produces macroscopic flow. The PLPC model conforms to the following assumptions: 1) The background porous medium is homogeneous and isotropic, and the horizontal directional arrangement of cracks in the medium causes anisotropy. 2) The boundary conditions between different layers are open, and the fluids can communicate with each other. 3) The aspect ratio of all the directional cracks in the medium is the same. 4) The entire analysis is limited to a long wavelength range, so the crack size and spacing are smaller than the wavelength.

In order to investigate the attenuation and dispersion of seismic waves caused by WIFF at different scales, the effect of the squirt fluid flow and the interlayer fluid flow on fluid pressure are first calculated, and then the constitutive equations and fluid pressure for the PLPC medium model are obtained by combining with Biot's equation. Finally, the corresponding wave equations are constructed to solve the wave velocities and attenuation factors of seismic waves.

2.1. Construction of the constitutive equations for periodic-layered porous-cracked media

The stress-strain relationship for anisotropic media is shown as follows (Biot, 1955):

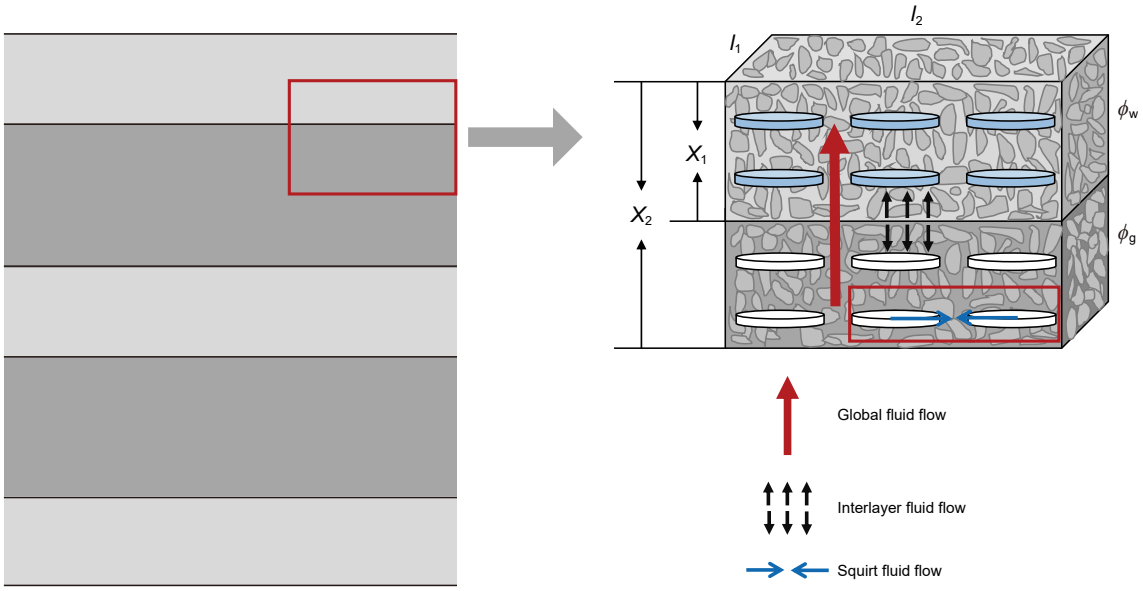

Fig. 1. Sketch of the periodic-layered porous-cracked media.

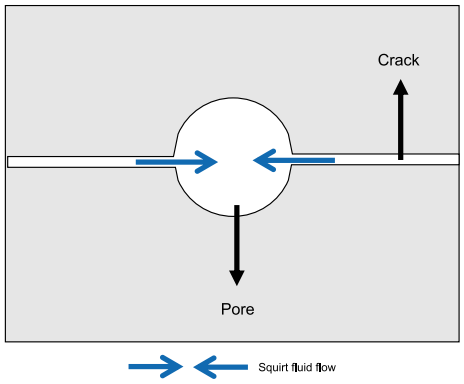

Fig. 2. Sketch of the annular-shaped crack.

$$\begin{bmatrix} \sigma^s_{xx} \\ \sigma^s_{yy} \\ \sigma^s_{zz} \\ \sigma^s_{yz} \\ \sigma^s_{xz} \\ \sigma^s_{xy} \\ -\phi P \end{bmatrix} = \begin{bmatrix} C_{11} & C_{12} & C_{13} & C_{14} & C_{15} & C_{16} & C_{17} \\ C_{12} & C_{22} & C_{23} & C_{24} & C_{25} & C_{26} & C_{27} \\ C_{13} & C_{23} & C_{33} & C_{34} & C_{35} & C_{36} & C_{37} \\ C_{14} & C_{24} & C_{34} & C_{44} & C_{45} & C_{46} & C_{47} \\ C_{15} & C_{25} & C_{35} & C_{45} & C_{55} & C_{56} & C_{57} \\ C_{16} & C_{26} & C_{36} & C_{46} & C_{56} & C_{66} & C_{67} \\ C_{17} & C_{27} & C_{37} & C_{47} & C_{57} & C_{67} & C_{77} \end{bmatrix} \begin{bmatrix} e_{xx} \\ e_{yy} \\ e_{zz} \\ e_{yz} \\ e_{xz} \\ e_{xy} \\ \Theta \end{bmatrix} \tag{1}$$

Eq. (1) is subjected to elementary deformation, and Θ is eliminated. Then, we can obtain

$$\sigma^s = Ae - \overline{\alpha}P \tag{2}$$

where $\sigma^s = \left(\sigma^s_{xx}, \sigma^s_{yy}, \sigma^s_{zz}, \sigma^s_{yz}, \sigma^s_{xz}, \sigma^s_{xy}\right)^{\mathrm{T}}$ denotes the solid-phase stress tensor, $e = (e_{xx}, e_{yy}, e_{zz}, e_{yz}, e_{xz}, e_{xy})^{\mathrm{T}}$ denotes the solid-phase strain tensor, $A_{ij} = C_{ij} - C_{i7}/C_{77}(i,j = 1,2,\cdots,6)$ denotes drained elastic coefficients, and the coefficient vector $\overline{\alpha} = (\overline{\alpha}_1, \overline{\alpha}_2, \overline{\alpha}_3, \overline{\alpha}_4, \overline{\alpha}_5, \overline{\alpha}_6)^{\mathrm{T}}$, in which $\overline{\alpha}_i = C_{i7}\phi/C_{77}, i = 1,2,\cdots,6$, P is the fluid pressure, and ϕ is porosity.

The total stress of the fluid-solid phase in this model can be expressed as

$$\begin{aligned} &\tau = \sigma^s - \phi P\delta_{ij}, \\ &\delta_{ij} = 0, i \neq j; \delta_{ij} = 1, i = j \end{aligned} \tag{3}$$

Substituting Eq. (2) into Eq. (3) yields

$$\tau = Ae - \alpha P \tag{4}$$

in which, $\alpha = \overline{\alpha} + \phi I$, and I is the unit matrix.

For porous VTI media, if the solid particles are assumed to be isotropic, the formula can be further simplified as

$$\begin{cases} \alpha_1 = \alpha_2 = 1 - \dfrac{C_{11} + C_{12} + C_{13}}{3K_s} \\ \alpha_3 = 1 - \dfrac{C_{13} + C_{23} + C_{33}}{3K_s} \\ \alpha_4 = \alpha_5 = \alpha_6 = 0 \end{cases} \tag{5}$$

in which, K_s represents the bulk modulus of solid grain. Thereby, the total stress of the novel model yields

$$\tau = Ce - \alpha P \tag{6}$$

in which $\tau = (\tau_{xx}, \tau_{yy}, \tau_{zz}, \tau_{yz}, \tau_{xz}, \tau_{xy})^{\mathrm{T}}$ denotes the total stress tensor, $e = (e_{xx}, e_{yy}, e_{zz}, e_{yz}, e_{xz}, e_{xy})^{\mathrm{T}}$ denotes the solid-phase strain tensor, C is a 6×6 matrix of elastic constants, and $\alpha = (\alpha_1, \alpha_2, \alpha_3, \alpha_4, \alpha_5, \alpha_6)^{\mathrm{T}}$ is the porous elastic coefficient tensor.

To more precisely analyze the attenuation and dispersion of micro-scale seismic waves due to the squirt fluid flow, Tang (2011) proposed a unified theory of elastic wave in porous and cracked media. Vertically oriented cracks are introduced into the rock, and then an annular-shaped pore-crack structure is form with the stiff pores in the background of the porous medium. In the unit rock volume, the increment of fluid dilatation into the porous space due to local fluid flow is q_v, and the pore pressure will also change accordingly with the added fluid content ϕq_v. Thus, the constitutive equation for the pore fluid pressure P is obtained (Tang et al., 2012):

$$P = -(\alpha\nabla\cdot\mathbf{u} + \nabla\cdot\mathbf{w} + \phi q_v)/\beta \tag{7}$$

where $\mathbf{w} = \phi(\mathbf{U} - \mathbf{u})$, $\mathbf{U}$ and $\mathbf{u}$ represent fluid displacement and

solid displacement respectively. $\beta = (\alpha - \phi)/K_s + \phi/K_f$, K_f represent the bulk modulus of pore fluid.

$S(\omega) = \phi q_v/P$ are used to characterize the effect of squirt fluid flow caused by the annular cracks on pore pressure, respectively. Eq. (7) can be rewritten as

$$P = -\frac{\phi F}{\phi + FS(\omega)}\left(\nabla \cdot \mathbf{U} + \frac{\alpha - \phi}{\phi}\nabla \cdot \mathbf{u}\right) \tag{8}$$

in which, $F = (1/K_f + 1/(\phi Q))^{-1}$ is Biot-flow coefficient, $1/Q = \alpha - \phi/K_s$.

The Biot-flow coefficient F is also not identical in the X-, Y-, Z-directions because of the directional effective stress. Thus, we define the Biot-flow coefficient tensor

$$F = \begin{pmatrix} F_1 & 0 & 0 \\ 0 & F_2 & 0 \\ 0 & 0 & F_3 \end{pmatrix} \tag{9}$$

where F_j denotes the Biot-flow tensor element in the j-direction, whose inverse F_j^{-1} reflects the compressibility of the Biot-flow to the solid-fluid coupled system, and

$$\begin{aligned} F_j &= \left(\frac{1}{K_f} + \frac{1}{\phi Q_j}\right)^{-1} \\ \frac{1}{Q_j} &= \frac{\alpha_j - \phi}{K_s} \end{aligned} \tag{10}$$

In addition, the expressions for $S(\omega)$ is

$$S(\omega) = \frac{\frac{8(1-\nu_0)d_c(1+\lambda)^3}{3\mu_0}\frac{1/K_0 - 1/K_s}{1/K_d - 1/K_0}M_c}{1 - \frac{3i\omega\eta(1+2\lambda)}{2K_f\lambda\gamma_c^2}\left[1 + \frac{4(1-\nu_0)K_f(1+\lambda)^3}{3\pi\mu_0\gamma_c(1+2\lambda)}M_c\right]} \tag{11}$$

Parameter M_c is given by

$$M_c = 1 + \frac{(4 - 5\nu_0)(R/a)^3}{2(7 - 5\nu_0)(1 + R/a)^3} + \frac{9(R/a)^5}{2(7 - 5\nu_0)(1 + R/a)^5} \tag{12}$$

in which, ν_0 is Poisson's ratio of background medium, μ and K_d represent the shear modulus and dry bulk modulus of solids, respectively, K_0 is the bulk modulus of saturated rock without the squirt flow. d_c and γ_c are crack density and crack aspect ratio respectively. $\lambda = R/a = [3\phi/(4\pi d_c)]^{1/3}$, R is the radius of the circular hole, a is the length of the crack. ω is frequency, and η is the fluid viscosity.

As the frequency tends to zero, $S(0)$ is a nonzero positive real number, which also leads to the low-frequency limit of the Tang's model constructed on the basis of the unified theory of micro-scale pore-crack media to be lower than the Gassmann limit. To correct this issue, the concept of dynamic bulk modulus was introduced (Yao et al., 2015). Therefore, the modified additional flexibility of the squirt flow $\Delta S(\omega)$ is

$$\Delta S(\omega) = S(\omega) - S(0) \tag{13}$$

in which $S(0) = \frac{8(1-\nu_0)d_c(1+\lambda)^3}{3\mu}\frac{1/K_0 - 1/K_s}{1/K_d - 1/K_0}M_c$.

White (1975) used the ideal layered model of with periodic alternation of water and gas layers to simulate the partial saturation of mesoscopic inhomogeneous fluid. In the PLPC medium, only the interlayer fluid flow caused by seismic waves propagation along the direction perpendicular to the layer is considered. In the periodic-layered medium, the interlayer fluid pressure difference caused by two adjacent layers with different fluids will cause interlayer fluid flow and affect the average fluid pressure. In the following, we derive the expression of fluid pressure considering interlayer fluid flow.

Considering that the unit rock contains two-layer media, the P-wave modulus of plane wave can be written as (White, 1975)

$$C_0 = \left(\frac{f_1}{M_1} + \frac{f_2}{M_2}\right)^{-1} \tag{14}$$

where

$$f_1 = \frac{X_1}{X_2}, f_2 = \frac{X_2 - X_1}{X_2} \tag{15}$$

M_1 and M_2 are the bulk modulus of P-wave in the upper and lower layers respectively, and

$$\begin{aligned} M_i &= \overline{M} + K_{Ai}\left(1 - \frac{K^*}{K_s}\right)^2 \\ \overline{M} &= K^* + \frac{4}{3}\mu_d \\ K_{Ai} &= \left(\frac{\phi}{K_{fi}} + \frac{1-\phi}{K_s} - \frac{K^*}{K_s^2}\right)^{-1} \\ K^* &= (C_{11} + 2C_{12} + 2C_{13} + 2C_{23} + C_{22} + C_{33})/9 \end{aligned} \tag{16}$$

In the research unit circled by the red frame in Fig. 1, when no fluid passes through the interface between the two layers, we assume that the pore fluid pressures of two-layer media are $P_1 e^{-i\omega t}$ and $P_2 e^{-i\omega t}$, respectively, which are expressed as a multiple of P_0:

$$\begin{aligned} P_1 e^{-i\omega t} &= T_1 P_0 e^{-i\omega t} \\ P_2 e^{-i\omega t} &= T_2 P_0 e^{-i\omega t} \end{aligned} \tag{17}$$

Since T_1 and T_2 are different, a pressure gradient will be generated at the interface, which will cause the fluid to flow between the layers, that is, the interlayer fluid flow. The velocity of the interlayer fluid flow is

$$V e^{-i\omega t} = \frac{P_1 - P_2}{Z_1 + Z_2} e^{-i\omega t} \tag{18}$$

in which, Z_1 and Z_2 represent the wave impedance in the upper and lower layers of the unit rock respectively, as follows,

$$\begin{aligned} Z_1 &= Z_{01}\coth(a_1 X_1) \\ Z_2 &= Z_{02}\coth(a_2(X_2 - X_1)) \end{aligned} \tag{19}$$

where $Z_{0i} = \sqrt{\eta_i K_{Ei}/(i\omega k)}$, $a_i = \sqrt{i\omega\eta_i/(K_{Ei}k)}$, k is the permeability.

K_{Ei} denotes the effective bulk modulus in the upper and lower layers of the unit rock,

$$K_{Ei} = K_{Ai}\frac{\overline{M}}{M_i} \tag{20}$$

Due to the interlayer fluid flow, the thickness of the two-layer medium changes dynamically. The variations are as follows:

$$\begin{aligned} U_1 e^{-i\omega t} &= \left(-Q_1\frac{V}{i\omega}\right)e^{-i\omega t} \\ U_2 e^{-i\omega t} &= \left(Q_2\frac{V}{i\omega}\right)e^{-i\omega t} \end{aligned} \tag{21}$$

where $V/(i\omega)$ is the displacement amplitude of the fluid flow

passing through the interface. The sum of the displacements is divided by the thickness to obtain the additional strain E_f due to interlayer fluid flow:

$$E_f e^{-i\omega t} = \left(\frac{U_1 + U_2}{X_2}\right) e^{-i\omega t} \tag{22}$$

According to White's theory, $T_1 = Q_1$ and $T_2 = Q_2$, T can be calculated as follows:

$$T_1 = \left(1 - \frac{K^*}{K_s}\right)\frac{K_{A1}}{M_1}; T_2 = \left(1 - \frac{K^*}{K_s}\right)\frac{K_{A2}}{M_2} \tag{23}$$

Finally, the additional strain E_f caused by the interlayer fluid flow can be obtained by substituting the calculated T and Eqs. (17), (18) and (21) into Eq. (22).

Thus, the total average pore fluid pressure in the PLPC medium can be obtained:

$$P = -\frac{\phi F}{\phi + F\left(S(\omega) + S_f\right)}\left(\nabla \cdot \mathbf{U} + \frac{\alpha - \phi}{\phi}\nabla \cdot \mathbf{u}\right) \tag{24}$$

where $S_f = E_f/P$ characterizes the effect of interlayer fluid flow on pore pressure.

2.2. Seismic wave velocities and attenuation factors for the periodic-layered porous-cracked media

The elastic kinetic equations based on microscopic fluid flow fields in porous anisotropic media are shown below:

$$\begin{cases} \dfrac{\partial \sigma_{xx}}{\partial x} + \dfrac{\partial \sigma_{xy}}{\partial y} + \dfrac{\partial \sigma_{xz}}{\partial z} = \dfrac{\partial^2}{\partial t^2}\left(\rho u_x + \rho_f w_x\right) \\ \dfrac{\partial \sigma_{xy}}{\partial x} + \dfrac{\partial \sigma_{yy}}{\partial y} + \dfrac{\partial \sigma_{yz}}{\partial z} = \dfrac{\partial^2}{\partial t^2}\left(\rho u_y + \rho_f w_y\right) \\ \dfrac{\partial \sigma_{xz}}{\partial x} + \dfrac{\partial \sigma_{yz}}{\partial y} + \dfrac{\partial \sigma_{zz}}{\partial z} = \dfrac{\partial^2}{\partial t^2}\left(\rho u_z + \rho_f w_z\right) \\ -\dfrac{\partial p}{\partial x_i} = \dfrac{\partial^2}{\partial t^2}\left(\rho_f u_i + \sum^{j} m_{ij} w_j\right) + \eta \sum^{j} \dfrac{1}{k_{ij}}\dfrac{\partial w_j}{\partial t} \end{cases} \tag{25}$$

in which $m_{11} = \left(\phi\rho_f + \rho_{ax}\right)/\phi^2$, $m_{22} = \left(\phi\rho_f + \rho_{ay}\right)/\phi^2$, $m_{33} = \left(\phi\rho_f + \rho_{az}\right)/\phi^2$, $\rho = (1-\phi)\rho_s + \phi\rho_f = \rho_1 + \rho_2$, $\rho_1 = (1-\phi)\rho_s$, $\rho_2 = \phi\rho_f$, and k_{ij} is the anisotropic permeability.

Substituting Eq. (6) into Eq. (25), the elastic wave propagation equation for periodic-layered porous-cracked media in general anisotropic conditions is obtained as follows:

$$\begin{cases} \dfrac{\partial}{\partial x_j}\left(C_{ijqp}\dfrac{\partial u_p}{\partial x_q}\right) - \dfrac{\partial}{\partial x_j}(\alpha_{ij}P) = \dfrac{\partial^2}{\partial t^2}(\rho_1 u_i + \rho_2 U_i) \\ -\dfrac{\partial P}{\partial x_i} = \dfrac{\partial^2}{\partial t^2}\left(\rho_f u_i + \sum^{j} m_{ij} w_j\right) + \eta \sum^{j} \dfrac{1}{\kappa_{ij}}\dfrac{\partial w_j}{\partial t} \end{cases} \tag{26}$$

Simplifying to the elastic wave equation for the PLPC medium is given by

$$\begin{aligned} & c_{11}\frac{\partial^2 u_x}{\partial x^2} + c_{66}\frac{\partial^2 u_x}{\partial y^2} + c_{44}\frac{\partial^2 u_x}{\partial z^2} + (c_{12} + c_{66})\frac{\partial^2 u_y}{\partial x \partial y} \\ & + (c_{13} + c_{44})\frac{\partial^2 u_z}{\partial x \partial z} - \alpha_1\frac{\partial P}{\partial x} = \frac{\partial^2}{\partial t^2}(\rho_1 u_x + \rho_2 U_x) \\ & c_{66}\frac{\partial^2 u_y}{\partial x^2} + c_{11}\frac{\partial^2 u_y}{\partial y^2} + c_{44}\frac{\partial^2 u_y}{\partial z^2} + (c_{12} + c_{66})\frac{\partial^2 u_x}{\partial x \partial y} + (c_{13} + c_{44})\frac{\partial^2 u_z}{\partial y \partial z} \\ & - \alpha_2\frac{\partial P}{\partial y} = \frac{\partial^2}{\partial t^2}(\rho_1 u_y + \rho_2 U_y) \\ & c_{44}\frac{\partial^2 u_z}{\partial x^2} + c_{44}\frac{\partial^2 u_z}{\partial y^2} + c_{33}\frac{\partial^2 u_z}{\partial z^2} + (c_{44} + c_{13})\frac{\partial^2 u_x}{\partial x \partial z} + (c_{44} + c_{13})\frac{\partial^2 u_y}{\partial y \partial z} \\ & - \alpha_3\frac{\partial P}{\partial z} = \frac{\partial^2}{\partial t^2}(\rho_1 u_z + \rho_2 U_z) \\ & -\frac{\partial P}{\partial x} = \frac{\partial^2}{\partial t^2}\left(\rho_f u_x + m_{11}\phi(U_x - u_x)\right) + \frac{\eta\phi}{k_{11}}\frac{\partial}{\partial t}(U_x - u_x) \\ & -\frac{\partial P}{\partial y} = \frac{\partial^2}{\partial t^2}\left(\rho_f u_y + m_{22}\phi(U_y - u_y)\right) + \frac{\eta\phi}{k_{22}}\frac{\partial}{\partial t}(U_y - u_y) \\ & -\frac{\partial P}{\partial z} = \frac{\partial^2}{\partial t^2}\left(\rho_f u_z + m_{33}\phi(U_z - u_z)\right) + \frac{\eta\phi}{k_{33}}\frac{\partial}{\partial t}(U_z - u_z) \\ & P = -\sum_{i=1}^{3}\frac{\phi F_i}{\phi + F_i\left(\Delta S(\omega) + S_f\right)}\left(\frac{\partial U_i}{\partial x_i} + \frac{\alpha_i - \phi}{\phi}e_{ii}\right) \end{aligned} \tag{27}$$

In order to eliminate the fluid displacement term of the above equation, the wave equation is only expressed by the solid displacement term and the fluid pressure term. Assume that,

$$\begin{aligned} u(x,y,z,t) &= u(x,y,z)e^{-i\omega t} \\ U(x,y,z,t) &= U(x,y,z)e^{-i\omega t} \\ P(x,y,z,t) &= P(x,y,z)e^{-i\omega t} \end{aligned} \tag{28}$$

Correspondingly, the wave propagation equation in the spatial-frequency domain of the proposed model is expressed as follows,

$$\begin{aligned} & \left(C_{11}\frac{\partial^2}{\partial x^2} + C_{66}\frac{\partial^2}{\partial y^2} + C_{44}\frac{\partial^2}{\partial z^2} + a_{11}\right)u_x + (C_{12} + C_{66})\frac{\partial^2 u_y}{\partial x \partial y} + (C_{13} + C_{44})\frac{\partial^2 u_z}{\partial x \partial z} - (\alpha_1 - \phi\theta_1)\frac{\partial P}{\partial x} = 0 \\ & (C_{12} + C_{66})\frac{\partial^2 u_x}{\partial x \partial y} + \left(C_{66}\frac{\partial^2}{\partial x^2} + C_{11}\frac{\partial^2}{\partial y^2} + C_{44}\frac{\partial^2}{\partial z^2} + a_{11}\right)u_y + (C_{13} + C_{44})\frac{\partial^2 u_z}{\partial y \partial z} - (\alpha_1 - \phi\theta_1)\frac{\partial P}{\partial y} = 0 \\ & (C_{44} + C_{13})\frac{\partial^2 u_x}{\partial x \partial z} + (C_{13} + C_{44})\frac{\partial^2 u_y}{\partial y \partial z} + \left(C_{44}\frac{\partial^2}{\partial x^2} + C_{44}\frac{\partial^2}{\partial y^2} + C_{33}\frac{\partial^2}{\partial z^2} + a_{33}\right)u_z - (\alpha_3 - \phi\theta_3)\frac{\partial P}{\partial z} = 0 \\ & \sum_i \frac{\phi F_i}{\phi + F_i\left(\Delta S(\omega) + S_f\right)}(\alpha_i - \phi\theta_i)\frac{\partial u_i}{\partial x_i} + \left[\phi\sum\frac{\phi F_i}{\phi + F_i\left(\Delta S(\omega) + S_f\right)}\frac{\theta_i}{\omega^2\rho_f}\frac{\partial^2}{\partial x_i^2} + 1\right]P = 0 \end{aligned} \tag{29}$$

in which,

$$\begin{aligned} &a_{jj} = \omega^2 \rho_j, \mathrm{j} = 1,2,3 \\ &\rho_j = \rho - \rho_2 \theta_j \\ &\theta_j = \left(\frac{\rho_{aj} \Big/ \rho_\mathrm{f} + \phi}{\phi} + i \frac{\eta \phi}{\omega \rho_\mathrm{f} k_{jj}} \right)^{-1} \end{aligned} \tag{30}$$

The plane-wave kernels of wave displacement components and pressure are given by

$$\begin{Bmatrix} u_x \\ u_y \\ u_z \\ P \end{Bmatrix} = \begin{Bmatrix} A_x \\ A_y \\ A_z \\ P_0 \end{Bmatrix} \exp\left[i(k_x x + k_y y + k_z z)k \right] \tag{31}$$

Substituting the above equation into Eq. (29) and organizing it gives

$$D \begin{bmatrix} A_x \\ A_y \\ A_z \\ P_0 \end{bmatrix} = 0 \tag{32}$$

in which

$$D = \begin{bmatrix} D_{11}k^2 - a_{11} & D_{12}k^2 & D_{13}k^2 & iD_{14}k \\ D_{21}k^2 & D_{22}k^2 - a_{22} & D_{23}k^2 & iD_{24}k \\ D_{31}k^2 & D_{32}k^2 & D_{33}k^2 - a_{33} & iD_{34}k \\ iD_{41}k & iD_{42}k & iD_{43}k & -D_{44}k^2 + 1 \end{bmatrix} \tag{33}$$

For the PLPC model, these variables in the matrix are

$$\begin{aligned} &a_{jj} = \omega^2 \rho_j, j = 1,2,3, a_{ij} = 0, i \neq j \\ &D_{11} = C_{11}k_x^2 + C_{66}k_y^2 + C_{44}k_z^2 \\ &D_{12} = D_{21} = (C_{12} + C_{66})k_x k_y \\ &D_{13} = D_{31} = (C_{13} + C_{44})k_x k_z \\ &D_{22} = C_{66}k_x^2 + C_{11}k_y^2 + C_{44}k_z^2 \\ &D_{23} = D_{32} = (C_{13} + C_{44})k_y k_z \\ &D_{33} = C_{44}k_x^2 + C_{44}k_y^2 + C_{33}k_z^2 \\ &D_{j4} = (\alpha_j - \phi\theta_j)k_j, j = 1,2,3 \\ &D_{4j} = \frac{\phi F_j}{\phi + F_j\left(\Delta S(\omega) + S_f\right)} \phi^{-1}(\alpha_j - \phi\theta_j)k_j, j = 1,2,3 \\ &D_{44} = \left(\frac{\phi F_1}{\phi + F_1\left(\Delta S(\omega) + S_\mathrm{f}\right)} \theta_1 k_x^2 + \frac{\phi F_2}{\phi + F_2\left(\Delta S(\omega) + S_\mathrm{f}\right)} \theta_2 k_y^2 + \frac{\phi F_3}{\phi + F_3\left(\Delta S(\omega) + S_\mathrm{f}\right)} \theta_3 k_z^2 \right) \Big/ \left(\omega^2 \rho_\mathrm{f}\right) \end{aligned} \tag{34}$$

By $\det(D) = 0$, yields

$$b_0 k^8 + b_1 k^6 + b_2 k^4 + b_3 k^2 + b_4 = 0 \tag{35}$$

The above equation is the wave number equation for the PLPC model, which in general has four different roots $k_2^i (i = 1,2,3,4)$, corresponding to four different waves.

In general, it is difficult to analyze the propagation properties of these waves in porous anisotropic rocks using the analytical solutions of the equations. Therefore, we only consider the properties of plane waves propagating in the XOZ plane here (other planes can be discussed by similar methods).

Let $k_x = \sin\theta, k_z = \cos\theta, k_y = 0$, then Eq. (33) can be simplified as

$$D = \begin{bmatrix} D_{11}k^2 - a_{11} & 0 & D_{13}k^2 & iD_{14}k \\ 0 & D_{22}k^2 - a_{22} & 0 & iD_{24}k \\ D_{31}k^2 & 0 & D_{33}k^2 - a_{33} & iD_{34}k \\ iD_{41}k & 0 & iD_{43}k & -D_{44}k^2 + 1 \end{bmatrix} \tag{36}$$

From $\det(D) = 0$, a root is obtained as

$$k_{\mathrm{SH}}^2 = \frac{a_{22}}{D_{22}} = \frac{\omega^2 \rho_y}{C_{66}\sin^2\theta + C_{44}\cos^2\theta} \tag{37}$$

Therefore, the phase velocity and attenuation of the SH-wave are

$$\begin{aligned} &v_{\mathrm{SH}} = \frac{\sqrt{C_{66}\sin^2\theta + C_{44}\cos^2\theta}}{\mathrm{Re}\left(\sqrt{\rho_y}\right)} \\ &Q_{\mathrm{SH}}^{-1} = 2\mathrm{Im}\left(\sqrt{\rho_y}\right) \Big/ \mathrm{Re}\left(\sqrt{\rho_y}\right) \end{aligned} \tag{38}$$

The remaining three roots are determined by the following equations:

$$\begin{aligned} &\det(D_1) = 0 \\ &D_1 = \begin{bmatrix} D_{11}k^2 - a_{11} & D_{13}k^2 & iD_{14}k \\ D_{13}k^2 & D_{33}k^2 - a_{33} & iD_{34}k \\ iD_{41}k & iD_{43}k & -D_{44}k^2 + 1 \end{bmatrix} \end{aligned} \tag{39}$$

The three roots of Eq. (39) correspond to the fast P-wave, the slow P-wave and the SV-wave, respectively. Wave number solutions are determined from the following equation:

$$c_0 k^6 + c_1 k^4 + c_2 k^2 + c_3 = 0 \tag{40}$$

where

$$\begin{aligned} c_0 &= -D_{11}D_{33}D_{44} + D_{13}^2 D_{44}, \\ c_1 &= D_{41}D_{14}D_{33} + D_{43}D_{34}D_{11} - D_{13}D_{43}D_{14} - D_{13}D_{41}D_{34} \\ &\quad + D_{11}D_{33} + D_{11}a_{33}D_{44} + a_{11}D_{33}D_{44} - D_{13}^2, \\ c_2 &= -D_{14}D_{41}a_{33} - a_{11}D_{43}D_{34} - a_{33}D_{11} - a_{11}D_{33} - a_{11}a_{33}D_{44}, \\ c_3 &= a_{11}a_{33}. \end{aligned} \tag{41}$$

Three coupled waves correspond to three wave number solutions $\tilde{k}_i (i = 1,2,3)$ of Eq. (40), respectively. The phase velocities and attenuation of these waves can be obtained directly from three complex wave number roots $\tilde{k}_i (i = 1,2,3)$ as

$$\begin{aligned} &v_i = \omega / \mathrm{Re}(\tilde{k}_i) \\ &Q_i^{-1} = 2\mathrm{Im}(\tilde{k}_i) \Big/ \mathrm{Re}(\tilde{k}_i) \end{aligned} \tag{42}$$

in which $\mathrm{Re}(k_i)$ represents the real part of the wave number, and $\mathrm{Im}(k_i)$ represents the imaginary part of the wave number.

Table 1
The rock physics parameters.

Parameter	Symbol	Value	Parameter	Symbol	Value
Grain bulk modulus	K_s, GPa	37.9	Grain density	ρ_s, kg·m^{-3}	2650
Grain shear modulus	μ_s, GPa	32.6	Water density	ρ_f, kg·m^{-3}	1000
Water bulk modulus	K_f, GPa	2.25	Gas density	ρ_g, kg·m^{-3}	70
Gas bulk modulus	K_g, GPa	9.6×10^{-3}	Crack density	d_c	0.025
Water viscosity	η_w, Pa•s	0.005	Crack aspect ratio	γ_c	0.0012
Gas viscosity	η_g, Pa•s	1×10^{-6}	Tortuosity	τ	2.4
Upper layer thickness	X_1, m	0.1	Upper layer porosity	ϕ_w	0.25
Total thickness	X_2, m	0.25	Sublayer porosity	ϕ_g	0.25
Coupling density	ρ_{ax}, kg·m^{-3}	300	Permeability	k_{xx}, mD	10
	ρ_{ay}, kg·m^{-3}	300		k_{yy}, mD	10
	ρ_{az}, kg·m^{-3}	100		k_{zz}, mD	20

3. Numerical example

In this section, we use the above method to calculate the dispersion, attenuation and frequency-dependent anisotropy of seismic waves in PLPC medium, and analyze the influence of different parameters on the dispersion and attenuation of seismic waves. Table 1 is the rock physics parameters to analyze the seismic wave theory.

The elastic modulus of the dry rock skeleton of the PLPC medium can be expressed as

$$\begin{aligned} C_{11}^0 &= (\lambda_d + 2\mu_d) - \lambda_d^2 \Delta N \big/ (\lambda_d + 2\mu_d) \\ C_{33}^0 &= (\lambda_d + 2\mu_d)(1 - \Delta N) \\ C_{13}^0 &= \lambda_d (1 - \Delta N) \\ C_{55}^0 &= \mu_d (1 - \Delta T) \\ C_{66}^0 &= \mu_d \end{aligned} \tag{43}$$

in which, $C_{23}^0 = C_{13}^0$, $C_{22}^0 = C_{11}^0$, $C_{44}^0 = C_{55}^0$, $C_{12}^0 = C_{11}^0 - 2C_{66}^0$, λ_d and μ_d are the Lamé constants of the dry rock. $\Delta N = 4d_c/[3g(1-g)]$, $\Delta T = 16d_c/[3(3-2g)]$, $g = \mu_d/(\lambda_d + 2\mu_d)$.

For fluid-containing anisotropic media, the generalized Gassmann equation can characterize the elastic modulus parameters of anisotropic media (Gassmann, 1951). Therefore, the elastic modulus of saturated rock in the three-scale model of the PLPC medium can be expressed as

$$\begin{aligned} C_{11} &= (\lambda + 2\mu) - \lambda^2 \Delta N \big/ (\lambda + 2\mu) + \alpha_{11}^2 M \\ C_{33} &= (\lambda + 2\mu)(1 - \Delta N) + \alpha_{33}^2 M \\ C_{13} &= \lambda(1 - \Delta N) + \alpha_{11}\alpha_{33} M \\ C_{55} &= \mu(1 - \Delta T) \\ C_{66} &= \mu \end{aligned} \tag{44}$$

in which, $C_{23} = C_{13}$, $C_{22} = C_{11}$, $C_{44} = C_{55}$, $C_{12} = C_{11} - 2C_{66}$. M is the Gassmann pore modulus,

$$M = \frac{K_s}{(1 - K^*/K_s) - \phi\left(1 - K_s/K_f\right)} \tag{45}$$

and K^* is generalized bulk modulus of dry rock,

$$K^* = \frac{1}{9}\sum_{i=1}^{3}\sum_{j=1}^{3} C_{ij}^0 \tag{46}$$

The P-wave velocity dispersion and attenuation curves of the three-scale model of anisotropic media with pores and cracks (red curve and dark blue curve) are compared with those of the fast P-wave velocity dispersion and attenuation curves given by the Biot theory based on VTI media (navy blue curve), the Tang theory with penny-shaped cracks (light blue curve) and annular-shaped cracks (yellow curve) considering macroscopic global flow, and the White periodic layered media theory (orange curve) considering macroscopic global flow. The crack density of the penny-shaped cracks (crack 1) is 0.025, and the crack aspect ratio is 0.0017; the crack density of the annular-shaped cracks (crack 2) is 0.025, and the

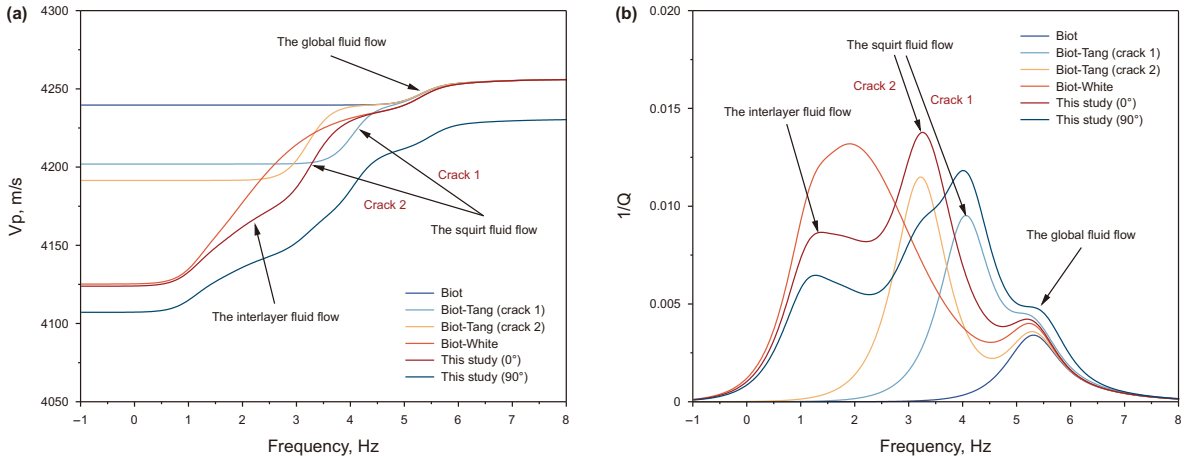

Fig. 3. Comparison of the dispersion **(a)** and attenuation **(b)** of the fast P-wave calculated with the proposed multi-scale wave theory with the existing theories.

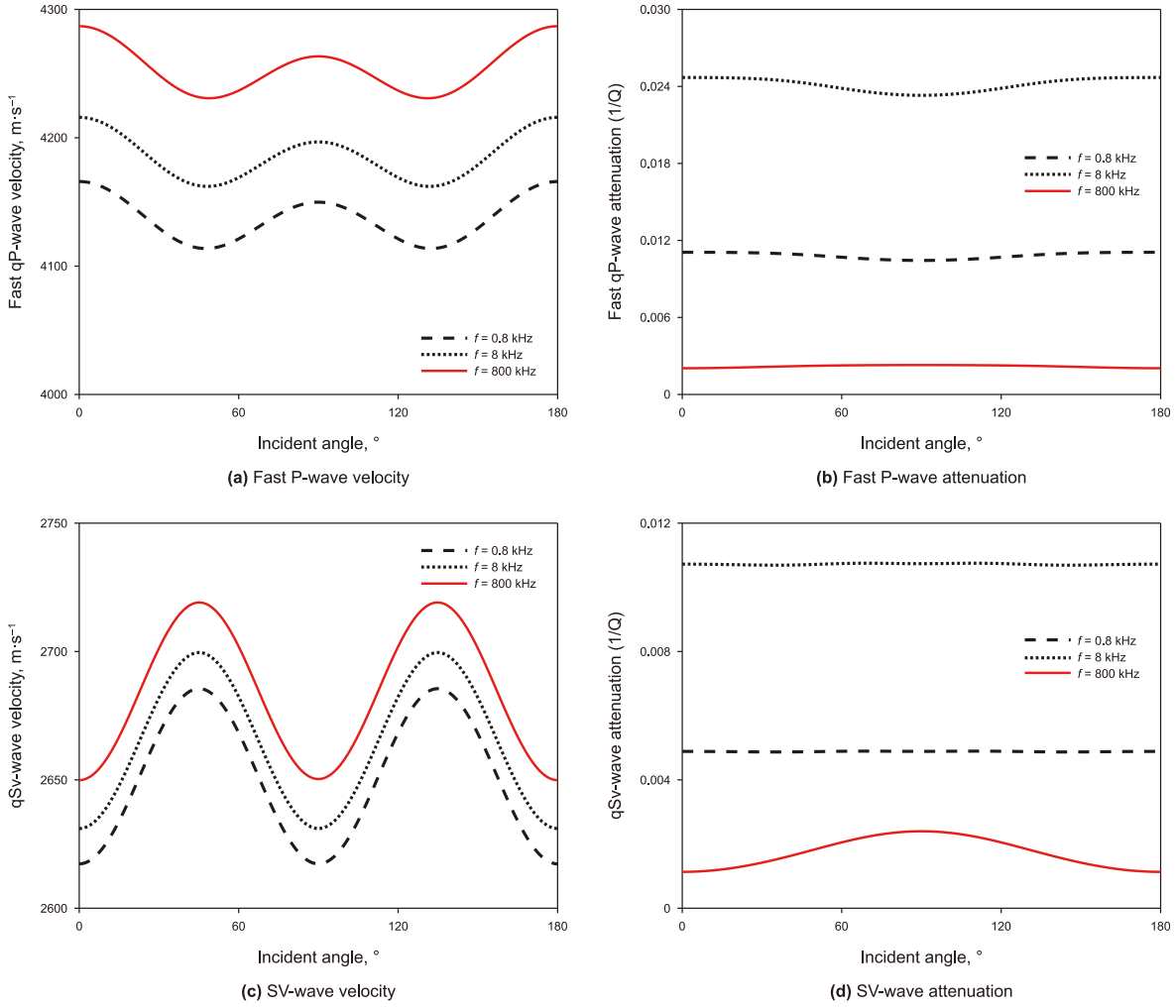

Fig. 4. Velocity of fast P-wave and SV-wave with propagation angle at different frequencies.

crack aspect ratio is 0.0017. The thickness of the upper medium is 0.15 m, and the anisotropic permeability of the fluid is 100 mD, and that of the fluid is 200 mD, and other parameters are shown in Table 1. As shown in Fig. 3, The interlayer fluid flow caused by the different saturated fluids in the upper and lower layers mainly occurs at 10^1–10^2 Hz, that is, the seismic frequency band. The squirt fluid flow caused by the microscopic cracks mainly occurs at 10^3–10^4 Hz, and the attenuation frequency of the annular-shaped cracks is lower than that of the penny-shaped cracks. The Biot global fluid flow mainly occurs in the high frequency band, that is, 10^5–10^6 Hz, and the attenuation and dispersion caused by it are relatively weak. Meanwhile, we can observe that the frequency band of the attenuation peak caused by each mechanism is consistent with the existing theory. However, due to the existence

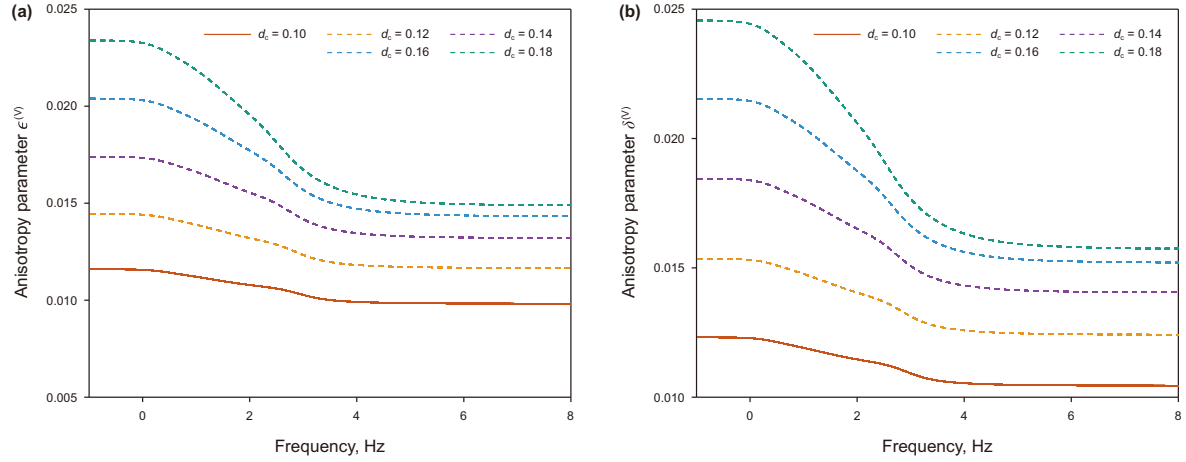

Fig. 5. Dispersion of anisotropy parameters in the model for wave propagation with different crack densities.

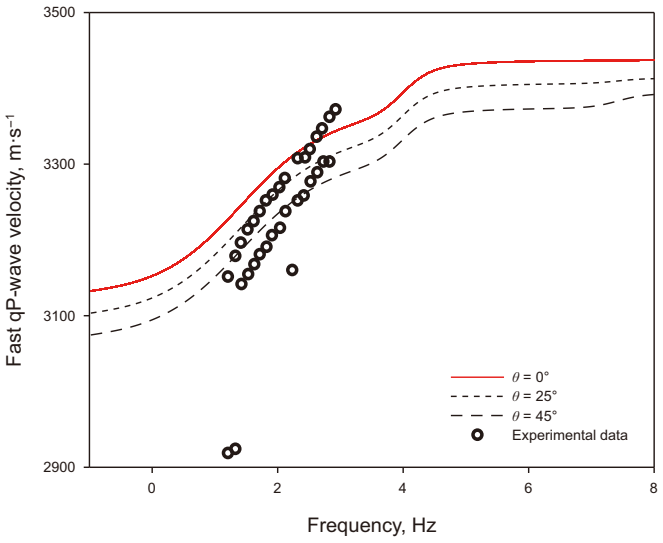

Fig. 6. Comparison of fast qP-wave velocities with experimental data.

of anisotropy, the velocity dispersion and attenuation of fast P-wave will change will change with the variation of the propagation angle, and this characteristic is the biggest difference between this theory and the theory of isotropic medium. The relative increase or decrease of the attenuation peak in different frequency bands may be due to the fact that different fluid flow mechanisms are not independent of each other. The interaction between them will affect the dispersion and attenuation caused by each WIFF mechanism.

To further investigate the rationality of the theory in this paper, we calculate the velocity curves of fast P-wave, slow P-wave and SV-wave with incident angle at frequencies of 0.8, 8 and 800 kHz. We assume that the incident angle θ is the angle between the propagation direction of the wave and the Z-axis. From Fig. 4, it is shown that the seismic wave velocity increases with the increase of frequency. Moreover, under the given medium model parameters, the velocities of fast P-wave and SV-wave show anisotropic characteristics. The SV-wave has its maximum velocity when its propagation direction is at an angle of 45° normal to the layer. The difference in the velocity values of the fast P-wave propagating along the parallel and perpendicular layer is not significant, which we attribute to the presence of interlayer fluid flow.

The Thomsen anisotropy parameters are calculated to better characterize the frequency-dependent anisotropy of seismic waves in PLPC medium, as follows (Thomsen, 1986):

$$\varepsilon^{(V)} = \frac{C_{11} - C_{33}}{2C_{33}},$$
$$\delta^{(V)} = \frac{(C_{13} + C_{44})^2 - (C_{33} - C_{44})^2}{2C_{33}(C_{33} - C_{44})}. \tag{47}$$

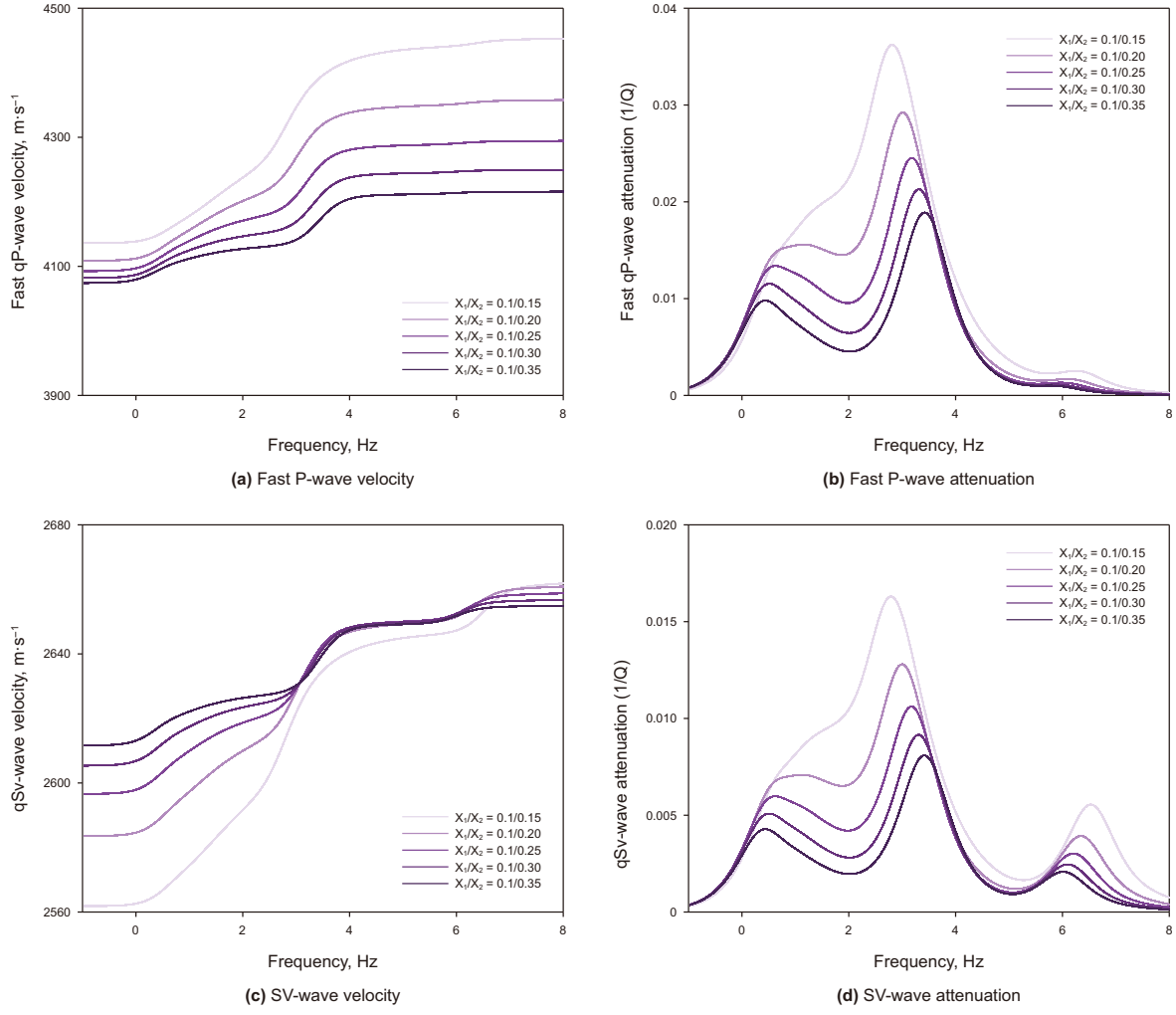

Fig. 7. Velocity dispersion and attenuation curves of fast P-wave and SV-wave in the PLPC model with different layer thickness ratios.

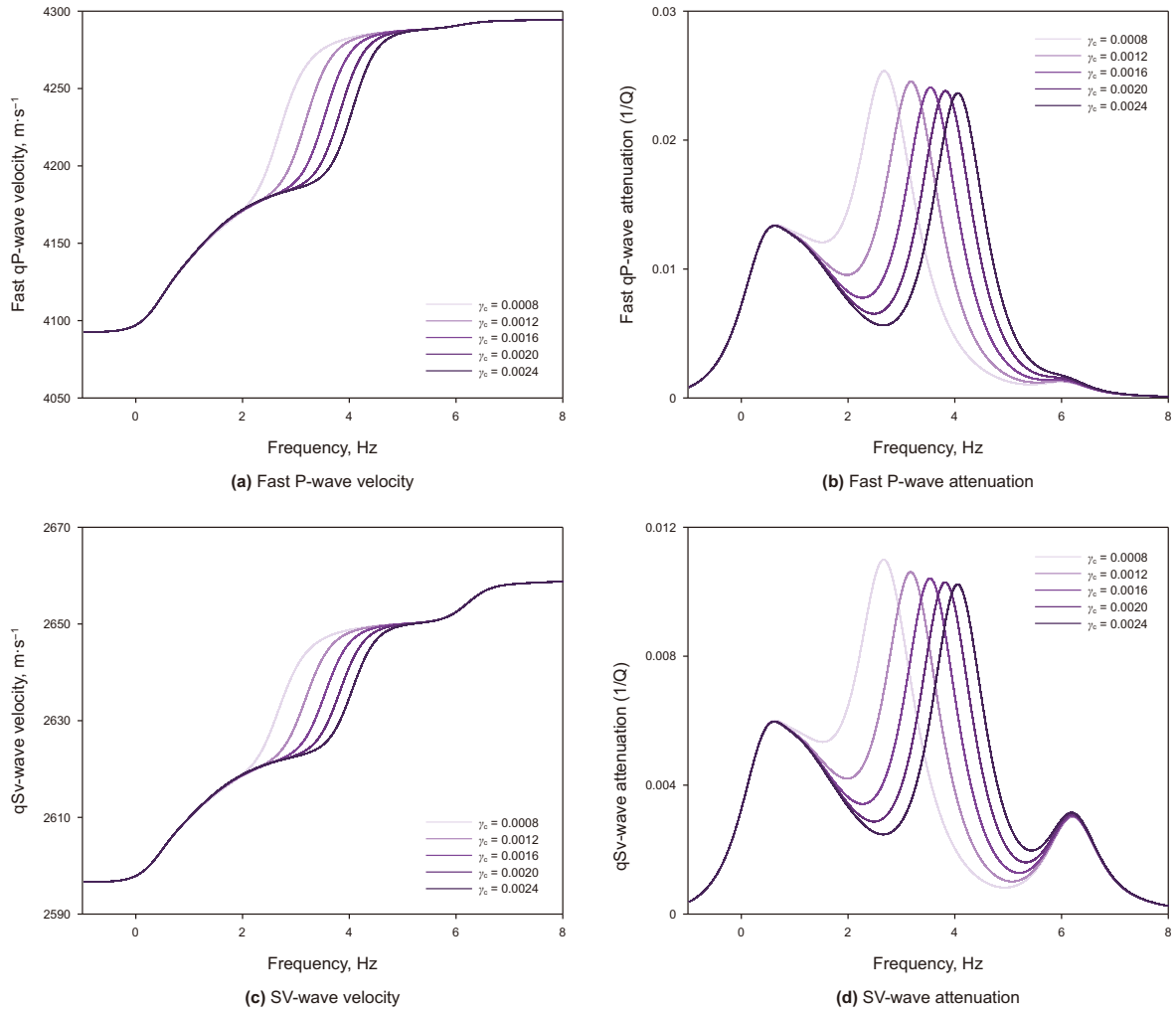

Fig. 8. Velocity dispersion and attenuation curves of fast P-wave and SV-wave in the PLPC model with different crack aspect ratios.

The characteristics of the Thomsen anisotropy parameters with frequency are analyzed for different crack densities, which are set at 0.1, 0.12, 0.14, 0.16 and 0.18, respectively. According to Fig. 5, the interlayer fluid flow and two kinds of squirt fluid flow will cause dispersion phenomenon to the anisotropic parameters in the frequency band below 10^4 Hz, which proves that the WIFF mechanism will also have a slight influence on the anisotropic parameters. Simultaneously, as the crack density increases, the anisotropic parameters also increase accordingly.

In order to verify the validity of the three-scale wave theory, a comparative analysis is conducted between the experimental data and the simulated fast P-wave velocities. The experimental data are fast P-wave velocities measured by low-frequency stress-strain experiments on water-saturated dense siltstone samples (Ba et al., 2017). The porosity of the tight siltstone is 0.14, the permeability is 0.084 mD, the rock background bulk modulus is 20 GPa, and the shear modulus is 11.8 GPa. The crack density of the annular-shaped crack in the model is set to 0.03, the crack aspect ratio is 0.002, the fluid viscosity is 0.001 Pa s, and the fluid bulk modulus is 2.25 GPa. From Fig. 6, the fast P-wave velocity dispersion phenomenon is obvious in the experimental data within the seismic frequency band of 10^1–10^3 Hz, and the theoretical P-wave velocity curve is consistent with the experimental data. The dispersion in the lower frequency band is caused by mesoscopic wave-induced flow, and the velocity curve shows multiple dispersion features. Therefore, the comparison of laboratory-measured velocities with theoretical predictions shows that the proposed three-scale wave-induced flow theory can better describe the frequency-dependent characteristics of the velocity.

Subsequently, the effects of different elastic parameters on the velocity dispersion and attenuation of the three seismic waves propagating along the *Z*-axis in the PLPC model are analyzed. The first is layer thickness ratio. We set the thickness of the upper layer to 0.1 m, and the thickness of the lower layer to 0.05, 0.10, 0.15, 0.20 and 0.25 m respectively. From Fig. 7, with the decrease of the layer thickness ratio, the attenuation value of the velocity shows an increasing trend. The variation of the layer thickness ratio has an effect on these WIFF mechanisms, with the attenuation frequency band of the squirt fluid flow shifting towards the low frequency direction, and the attenuation frequency band of the interlayer fluid flow and the global fluid flow shifting towards the high frequency direction.

As shown in Fig. 8, the dispersion attenuation under different crack aspect ratios is analyzed. The aspect ratios of the annular cracks in the upper and lower media are set to 0.008, 0.0012, 0.0016, 0.002 and 0.0024, respectively. The variation of the crack aspect ratio mainly affects the microscopic squirt fluid flow mechanism. With the increase of the crack aspect ratio, the velocity

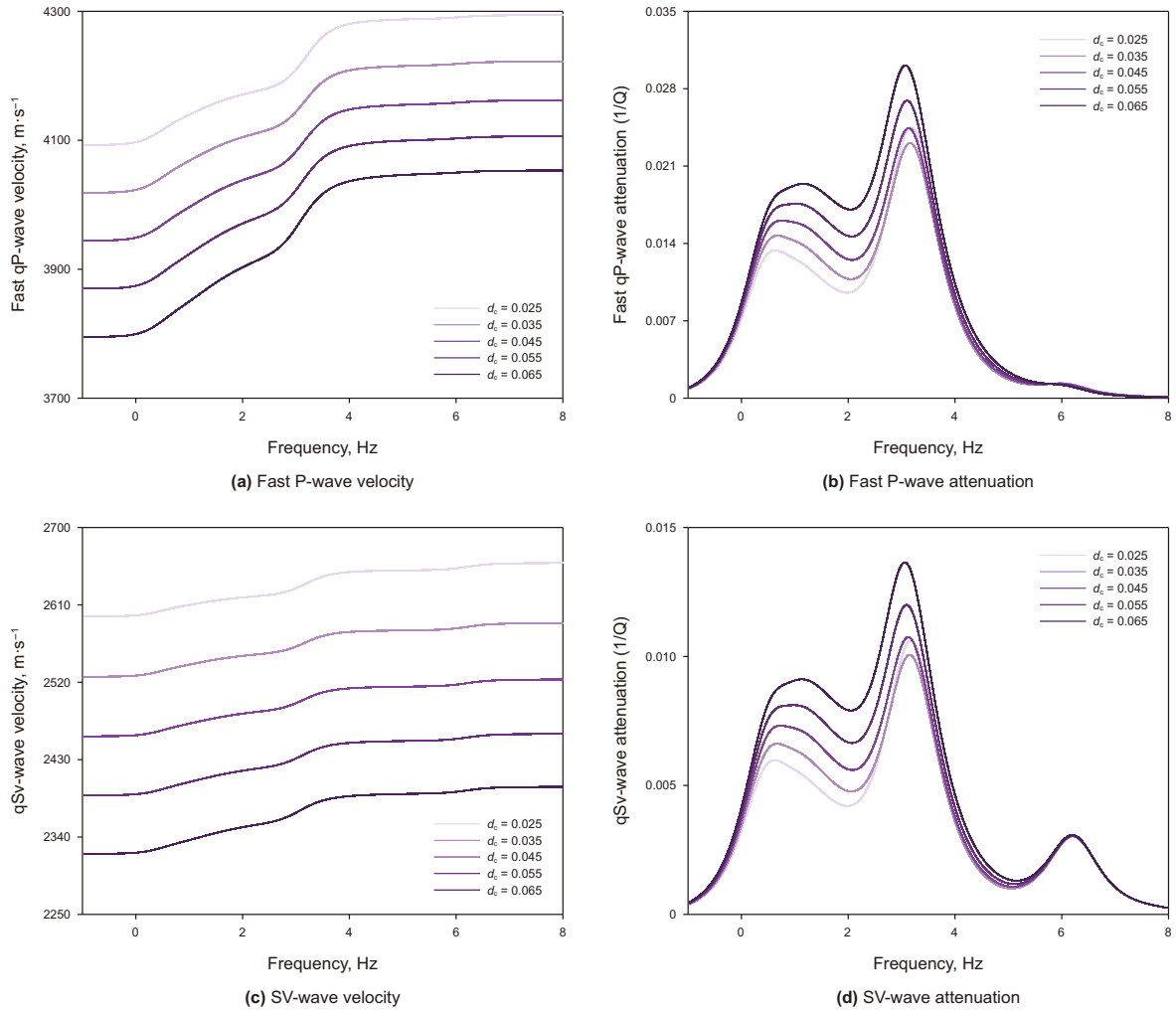

Fig. 9. Velocity dispersion and attenuation curves of fast P-wave and SV-wave in the PLPC model with different crack densities.

of two seismic waves decreases relatively, the attenuation frequency band moves to the high frequency direction, and the attenuation peak does not change significantly.

The crack density also has a significant effect on seismic wave velocity and dispersion. We set the crack densities of the annular-shaped cracks are 0.025, 0.035, 0.045, 0.055 and 0.065, respectively. According to Fig. 9, the crack density mainly affects the microscopic squirt fluid flow mechanism and the mesoscopic interlayer fluid flow mechanism. With the increase of crack density, the velocity of seismic wave decreases, the attenuation peak increases, and the attenuation frequency band is not affected.

Finally, we analyze the influence mechanism of different permeability on seismic wave velocity and dispersion. Here we set the permeability in the *X*- and *Y*-axis directions to be 10, 20, 100, 200 and 400 mD, and the permeability in the *Z*-axis direction to be 5, 10, 50, 100 and 200 mD. As shown in Fig. 10, the variation of permeability has little effect on the total attenuation of seismic waves and mainly affects the mesoscopic interlayer fluid flow and macroscopic Biot fluid flow mechanisms. When the permeability increases, the attenuation peak characterizing the interlayer fluid flow moves to the high frequency direction, and the attenuation peak characterizing the Biot fluid flow moves to the low frequency direction.

4. Conclusion

In this work, a periodic-layered porous medium is modeled in which each layer is an anisotropic background saturated with different fluids and contains the annular-shaped cracks, termed as the PLPC medium model. This model incorporates three WIFF mechanisms: microscopic squirt fluid flow, mesoscopic interlayer fluid flow and macroscopic Biot fluid flow. By means of the Biot's poroelasticity theory, the wave equations are derived by constructing the constitutive matrix, fluid pressure equation and motion differential equation of the PLPC medium. By assuming the plane wave solution and solving the Christoffel equation, the corresponding seismic wave velocity and attenuation factor are obtained, and the Thomsen anisotropic parameters are further calculated. Subsequently, the velocity dispersion and attenuation of seismic waves due to multi-scale WIFF mechanisms are investigated at different incident angles. The analysis shows that three types of WIFF mechanisms are dominant on different frequency bands of seismic waves, and the interlayer fluid flow mechanism mainly occurs in the seismic frequency band, which has potential guiding significance for subsequent oil/gas identification and reservoir prediction. Meanwhile, the novel model also demonstrates the significant frequency-dependent anisotropy characteristics. The maximum dispersion of P-wave occurs in the direction perpendicular to the layer, while the maximum dispersion of SV-

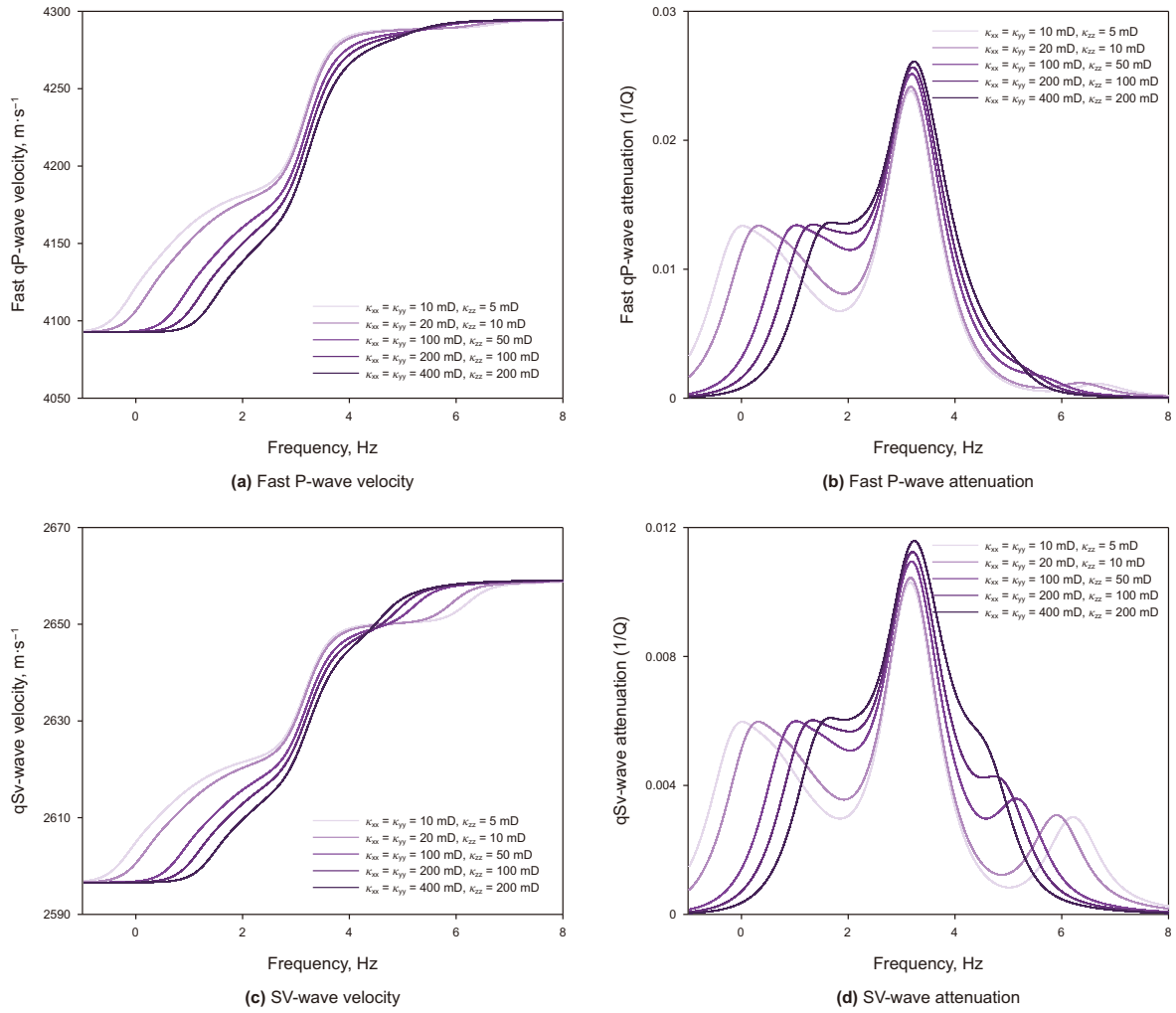

Fig. 10. Velocity dispersion and attenuation curves of fast P-wave and SV-wave in the PLPC model with different permeabilities.

wave occurs in the direction with the incident angle of around 45°. The results show that the parameters such as layer thickness ratio, crack aspect ratio and crack density have an impact on the dispersion and attenuation of seismic waves. Each elastic parameter controls the WIFF mechanism differently, mainly affecting the attenuation peak, attenuation frequency band and velocity. Based on the proposed three-scale theoretical model, the influence of different elastic parameters on velocity dispersion, attenuation and frequency-dependent anisotropy characteristics can be analyzed to optimize sensitivity parameters for subsequent seismic reflection characteristics research. Furthermore, this study can also provide a theoretical basis for the matching of logging data and seismic data, thereby improving the effectiveness and stability of reservoir prediction.

CRediT authorship contribution statement

Zhao-Yun Zong: Writing – review & editing, Writing – original draft, Visualization, Validation, Software, Methodology, Investigation, Formal analysis, Conceptualization. **Yan-Wen Feng:** Writing – review & editing, Validation, Supervision, Resources, Methodology, Data curation, Conceptualization. **Fu-Bin Chen:** Writing – review & editing, Writing – original draft, Visualization, Validation, Supervision, Software, Methodology, Investigation, Formal analysis. **Guang-Zhi Zhang:** Liu Yang, Data curation, Funding acquisition, Resources, Validation, Writing – review & editing.

Data availability statement

The data underlying this article will be shared on reasonable request to the corresponding author.

Declaration of competing interest

The authors declare no conflict of interest.

Acknowledgements

The authors cordially thank the sponsorship of the National Natural Science Foundation of China (U24B2020, 42174139).

References

Amalokwu, K., Best, A.I., Chapman, M., 2016. Effects of aligned fractures on the response of velocity and attenuation ratios to water saturation variation: a laboratory study using synthetic sandstones. Geophys. Prospect. 64 (4), 942–957. https://doi.org/10.1111/1365-2478.12378.

Ba, J., Carcione, J., Nie, J., 2011. Biot-Rayleigh theory of wave propagation in double-porosity media. J. Geophys. Res. 116, B06202. https://doi.org/10.1029/2010JB008185.

Ba, J., Xu, W., Fu, L.Y., et al., 2017. Rock anelasticity due to patchy saturation and fabric heterogeneity: a double double-porosity model of wave propagation.

J. Geophys. Res. Solid Earth 122 (3), 1949–1976. https://doi.org/10.1002/2016JB013882.
Batzle, M., Han, D.H., Castagna, J.P., 2001. Fluids and frequency dependent seismic velocity of rocks. Geophysics 20, 5–8. https://doi.org/10.1190/1.1438900.
Biot, M.A., 1955. Theory of elasticity and consolidation for a porous anisotropic solid. J. Appl. Phys. 26, 182–185. https://doi.org/10.1063/1.1721956.
Biot, M.A., 1956a. Theory of propagation of elastic waves in a fluid-saturated porous solid. I. Low-frequency range. J. Acoust. Soc. Am. 28, 168–178. https://doi.org/10.1121/1.1908239.
Biot, M.A., 1956b. Theory of propagation of elastic waves in a fluid-saturated porous solid. II. Higher frequency range. J. Acoust. Soc. Am. 28, 179–191. https://doi.org/10.1121/1.1908241.
Chapman, M., 2003. Frequency-dependent anisotropy due to meso-scale fractures in the presence of equant porosity. Geophys. Prospect. 51, 369–379. https://doi.org/10.3997/2214-4609-pdb.5.P033.
Chapman, M., 2009. Modeling the effect of multiple sets of mesoscale fractures in porous rock on frequency-dependent anisotropy. Geophysics 74, D97–D103. https://doi.org/10.1190/1.3204779.
Chen, F.B., Zong, Z.Y., Yin, X.Y., 2022a. Acoustothermoelasticity for joint effects of stress and thermal fields on wave dispersion and attenuation. J. Geophys. Res. Solid Earth 127, e2021JB023671. https://doi.org/10.1029/2021JB023671.
Chen, Y., Zong, Z.Y., Zhu, H.J., 2022b. Biot-spherical squirt (BISSQ) model for wave attenuation and dispersion. Geophys. J. Int. 231 (2), 1138–1149. https://doi.org/10.1093/gji/ggac250.
Chen, F.B., Zong, Z.Y., Yin, X.Y., et al., 2023. Pressure and frequency dependence of elastic moduli of fluid-saturated dual-porosity rocks. Geophys. Prospect. 71, 1599–1615. https://doi.org/10.1111/1365-2478.13395.
Diallo, M.S., Prasad, M., Appel, E., 2003. Comparison between experimental results and theoretical predictions for P-wave velocity and attenuation at ultrasonic frequency. Wave Motion 37 (1), 1–16. https://doi.org/10.1016/S0165-2125(02)00018-5.
Dutta, N.C., Ode, H., 1979. Attenuation and dispersion of compressional waves in fluid-filled porous rocks with partial gas saturation (White model)—Part II: results. Geophysics 44, 1789–1805. https://doi.org/10.1190/1.1440939.
Dvorkin, J., Mavko, G., Nur, A., 1995. Squirt flow in fully saturated rocks. Geophysics 60, 97–107. https://doi.org/10.1190/1.1443767.
Gassmann, F., 1951. Elastic waves through a packing of spheres. Geophysics 16 (4), 673–685. https://doi.org/10.1190/1.1437718.
Guo, J.X., Han, T.C., Fu, L.Y., et al., 2019. Effective elastic properties of rocks with transversely isotropic background permeated by aligned penny-shaped cracks. J. Geophys. Res. Solid Earth 124, 400–424. https://doi.org/10.1029/2018JB016412.
Gurevich, B., Lopatnikov, S.L., 1995. Velocity and attenuation of elastic waves in finely layered porous rocks. Geophys. J. Int. 121, 933–947. https://doi.org/10.1111/j.1365-246X.1995.tb06449.x.
Gurevich, B., Makarynska, D., de Paula, O.B., et al., 2010. A simple model for squirt-flow dispersion and attenuation in fluid-saturated granular rocks. Geophysics 75, N109–N120. https://doi.org/10.1190/1.3509782.
Hudson, J.A., Liu, E., Crampin, S., 1996. The mechanical properties of materials with interconnected cracks and pores. Geophys. J. Int. 124, 105–112. https://doi.org/10.1111/j.1365-246X.1996.tb06355.x.
Kong, L.Y., Gurevich, B., Müller, T.M., et al., 2013. Effect of fracture fill on seismic attenuation and dispersion in fractured porous rocks. Geophys. J. Int. 195, 1679–1688. https://doi.org/10.1093/gji/ggt354.
Krzikalla, F., Müller, T.M., 2011. Anisotropic P-SV-wave dispersion and attenuation due to inter-layer flow in thinly layered porous rocks. Geophysics 76, WA135–WA145. https://doi.org/10.1190/1.3555077.
Li, X.B., Yan, J.G., 2023. Characteristics of dispersion and attenuation with a unified multiscale model in porous medium containing saturated fluid and multiscale fractures. Geophysics 88, MR83–MR93. https://doi.org/10.1190/geo2022-0410.1.
Li, L., Yan, S.H., Liu, Q.M., et al., 2018a. Micro- and macroscopic study of crack propagation in coal: theoretical and experimental results and engineering practice. J. Geophys. Eng. 15, 1706–1718. https://doi.org/10.1088/1742-2140/aabb34.
Li, S.G., Du, X.H., Zhao, P.X., et al., 2018b. Experimental study on crack evolution characteristics of rock-like materials under different strain rates. J. Geophys. Eng. 15, 2071–2078. https://doi.org/10.1088/1742-2140/aabb66.
Liao, J.P., Wen, P., Guo, J.X., et al., 2023. Seismic dispersion, attenuation and frequency-dependent anisotropy in a fluid-saturated porous periodically layered medium. Geophys. J. Int. 234, 331–345. https://doi.org/10.1093/gji/ggad080.
Lissa, S., Barbosa, N.D., Rubino, J.G., et al., 2019. Seismic attenuation and dispersion in poroelastic media with fractures of variable aperture distributions. Solid Earth 10, 1321–1336. https://doi.org/10.5194/se-10-1321-2019.
Mavko, G.M., Nur, A., 1979. Wave attenuation in partially saturated rocks. Geophysics 44, 161–178. https://doi.org/10.1190/1.1440958.
Meng, H., Wei, Z.T., 2021. Frequency-dependent elastic wave propagation through anisotropic media induced by saturated cracks. Arab. J. Geosci. 14, 2031. https://doi.org/10.1007/s12517-021-07027-0.
Mukerji, T., Mavko, G., 1994. Pore fluid effects on seismic velocity in anisotropic rocks. Geophysics 59, 233–244. https://doi.org/10.1190/1.1443585.
Müller, T.M., Gurevich, B., Lebedev, M., 2010. Seismic wave attenuation and dispersion resulting from wave-induced flow in porous rocks—a review. Geophysics 75, 75A147–175A164. https://doi.org/10.1190/1.3463417.
Pang, S., Stovas, A., 2020. Low-frequency anisotropy in fractured and layered media. Geophys. Prospect. 68, 353–370. https://doi.org/10.1111/1365-2478.12833.
Parra, J.O., Xu, P.C., 1994. Dispersion and attenuation of acoustic guided waves in layered fluid-filled porous media. J. Acoust. Soc. Am. 95, 91–98. https://doi.org/10.1121/1.408269.
Pride, S., Berryman, J., Harris, J., 2004. Seismic attenuation due to wave-induced flow. J. Geophys. Res. 109, B01201. https://doi.org/10.1029/2003JB002639.
Sayers, C.M., Kachanov, M., 1995. Microcrack-induced elastic wave anisotropy of brittle rocks. J. Geophys. Res. Solid Earth 100, 4149–4156. https://doi.org/10.1029/94JB03134.
Sharma, M.D., 2004. Wave propagation in a general anisotropic poroelastic medium with anisotropic permeability: phase velocity and attenuation. Int. J. Solid Struct. 41, 4587–4597. https://doi.org/10.1016/j.ijsolstr.2004.02.066.
Sharma, M.D., 2007. Wave propagation in a general anisotropic poroelastic medium: Biot's theories and homogenisation theory. J. Earth Syst. Sci. 116, 357–367. https://doi.org/10.1007/s12040-007-0033-3.
Shuai, D., Stovas, A., Wei, J.X., et al., 2020. Frequency-dependent anisotropy due to two orthogonal sets of mesoscale fractures in porous media. Geophys. J. Int. 221, 1450–1467. https://doi.org/10.1093/gji/ggaa081.
Solovyev, S., Novikov, M., Lisitsa, V., 2023. A numerical investigation of wave-induced fluid flows in anisotropic fractured porous media. Comput. Math. Appl. 140, 78–88. https://doi.org/10.1016/j.camwa.2023.03.013.
Subramaniyan, S., Quintal, B., Madonna, C., et al., 2015. Laboratory-based seismic attenuation in Fontainebleau sandstone: evidence of squirt flow. J. Geophys. Res. Solid Earth 120, 7526–7535. https://doi.org/10.1002/2015JB012290.
Sun, W.T., 2021. On the theory of Biot-patchy-squirt mechanism for wave propagation in partially saturated double-porosity medium. Phys. Fluids 33, 076603. https://doi.org/10.1063/5.0057354.
Sun, W.T., Ba, J., Carcione, J.M., 2016. Theory of wave propagation in partially saturated double-porosity rocks: a triple-layer patchy model. Geophys. J. Int. 205, 22–37. https://doi.org/10.1093/gji/ggv551.
Tang, X.M., 2011. A unified theory for elastic wave propagation through porous media containing cracks—an extension of Biot's poroelastic wave theory. Sci. China Earth Sci. 6, 784–795. https://doi.org/10.1007/s11430-011-4245-7.
Tang, X.M., Chen, X.L., Xu, X.K., 2012. A cracked porous medium elastic wave theory and its application to interpreting acoustic data from tight formations. Geophysics 77, D245–D252. https://doi.org/10.1190/geo2012-0091.1.
Thomsen, L., 1986. Weak elastic anisotropy. Geophysics 51, 1954–1966. https://doi.org/10.1190/1.1442051.
Wang, X.Q., Ge, H.K., Han, P., 2018. A new model for fracability evaluation with consideration of natural cracks. J. Geophys. Eng. 15, 1492–1505. https://doi.org/10.1088/1742-2140/aab500.
Wang, Y.R., Zong, Z.Y., Yin, X.Y., 2022. Fluid discrimination incorporating amplitude variation with angle inversion and squirt flow of the fluid. Petrol. Sci. 19, 1592–1604. https://doi.org/10.1016/j.petsci.2022.03.007.
Wang, Y.R., Zong, Z.Y., Sun, Q.H., 2023. Modeling the effect of multi-scale heterogeneities on wave attenuation and velocity dispersion. IEEE Trans. Geosci. Rem. Sens. 61, 1–17. https://doi.org/10.1109/TGRS.2023.3244654.
Wei, J.X., Di, B.R., Ding, P.B., 2013. Effect of crack aperture on P-wave velocity and dispersion. Appl. Geophys. 10 (2), 125–133. https://doi.org/10.1007/s11770-013-0379-z.
White, J.E., 1975. Computed seismic speeds and attenuation in rocks with partial gas saturation. Geophysics 40, 224–232. https://doi.org/10.1190/1.1440520.
White, J.E., Mihailova, N., Lyakhovitsky, F., 1975. Low-frequency seismic waves in fluid-saturated layered rocks. J. Acoust. Soc. Am. 57, S30. https://doi.org/10.1121/1.1995164.
Wu, C.F., Ba, J., Carcione, J.M., et al., 2020. A squirt-flow theory to model wave anelasticity in rocks containing compliant microfractures. Phys. Earth Planet. In. 301, 106450. https://doi.org/10.1016/j.pepi.2020.106450.
Xu, D.H., Han, T.C., Fu, L.Y., 2021. Frequency-dependent seismic properties in layered and fractured rocks with partial saturation. Geophys. Prospect. 69, 1716–1732. https://doi.org/10.1111/1365-2478.13133.
Xu, M.M., Yin, X.Y., Zong, Z.Y., 2022. Wave dispersion and attenuation due to multi-scale wave-induced fluid flow in layered partially saturated pore-crack media. J. Pet. Sci. Eng. 208, 109447. https://doi.org/10.1016/j.petrol.2021.109447.
Yang, D.H., Zhang, Z.J., 2002. Poroelastic wave equation including the Biot/squirt mechanism and the solid/fluid coupling anisotropy. Wave Motion 35, 223–245. https://doi.org/10.1016/S0165-2125(01)00106-8.
Yao, Q.L., Han, D.H., Yan, F.Y., et al., 2015. Modeling attenuation and dispersion in porous heterogeneous rocks with dynamic fluid modulus. Geophysics 80 (3), D183–D194. https://doi.org/10.1190/geo2013-0410.1.
Zhang, J.W., Huang, H.D., Zhu, B.H., et al., 2017. Fluid identification based on P-wave anisotropy dispersion gradient inversion for fractured reservoirs. Acta Geophys. 65, 1081–1093. https://doi.org/10.1007/s11600-017-0088-8.
Zhang, F.C., Lu, Y.W., Sang, K.H., et al., 2019. Attenuation and dispersion of seismic waves in a cracked-fractured medium. Chin. J. Geophys. 62, 3164–3174. https://doi.org/10.6038/cjg2019M0216.